An Exchange-Coupled Donor Molecule in Silicon

M. F. Gonzalez-Zalba,*[∥,†] André Saraiva,*[‡,#] María J. Calderón,[§] Dominik Heiss,[†,⊥] Belita Koiller,[‡] and Andrew J. Ferguson[†]

[†]Cavendish Laboratory, University of Cambridge, J.J. Thomson Avenue, Cambridge CB3 0HE, U.K.
[‡]Instituto de Fisica, Universidade Federal do Rio de Janeiro, Caixa Postal 68528, 21941-972 Rio de Janeiro, Brazil
[§]Instituto de Ciencia de Materiales de Madrid, ICMM-CSIC, Cantoblanco, E-28049 Madrid, Spain
[∥]Hitachi Cambridge Laboratory, JJ Thomson Ave, Cambridge CB3 0HE, U.K.
[⊥]Eindhoven University of Technology, 5612 AZ Eindhoven, The Netherlands
[#]University of Wisconsin-Madison, Madison, Wisconsin 53706, United States

S *Supporting Information*

ABSTRACT: We present a combined experimental−theoretical demonstration of the energy spectrum and exchange coupling of an isolated donor pair in a silicon nanotransistor. The molecular hybridization of the atomic orbitals leads to an enhancement of the one- and two-electron binding energies and charging energy with respect to the single donor case, a desirable feature for quantum electronic devices. Our hydrogen molecule-like model based on a multivalley central-cell corrected effective mass theory incorporating a full configuration interaction treatment of the 2-electron spectrum matches the measured data for an arsenic diatomic molecule with interatomic distance $R = 2.3 \pm 0.5$ nm.

KEYWORDS: *Quantum computing, quantum chemistry, silicon, dopants, transistor, exchange coupling*
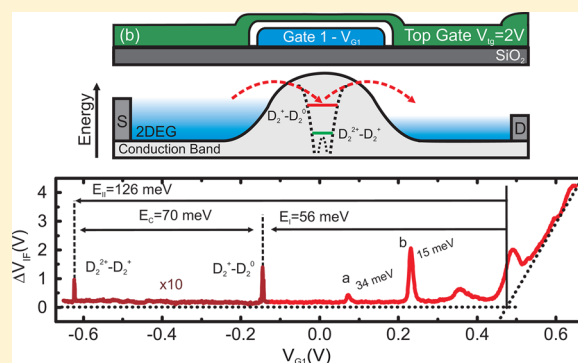
Donors in silicon, conceptually described as hydrogen atom analogues in a semiconductor environment, have become a key ingredient of many "More-than-Moore" proposals such as quantum information processing[1−5] and single-dopant electronics.[6,7] The level of maturity this field has reached has enabled the fabrication and demonstration of transistors that base their functionality on a single impurity atom,[8−10] opening up a window for fundamental innovation. In that sense, single dopants have been detected via resonant transport in the subthreshold regime of nanoFETs,[11−13] and recently a single-atom transistor has been fabricated deterministically.[9] Experimental studies have been backed up by theoretical calculations that explained deviations from the donor bulk energy spectrum. Capacitive coupling to the gate electrodes,[11] electric-field-induced Stark shift,[14] and dielectric confinement[15] modify the one and two-electron binding energies and reduce the charging energy presenting a challenge for future technologies in terms of reproducibility and elevated temperature operation.

Two-donor devices present an opportunity to harness the potential of single donor technology. In that direction, researchers have developed donor-based single-electron pumps[16−18] and studied fundamental properties of donors such as valley-orbit splitting,[19] Anderson−Mott transition,[20] and coherent coupling.[21] Very recently, exchange coupled multi-donor quantum dots with a few electrons have been reported.[22] However, the most appealing implementation is quantum computation where, in the Kane model, a donor molecule forms a basic unit of quantum information processing.[1,23]

Here we present a combined experimental−theoretical demonstration of the energy spectrum of a strongly interacting donor pair in the channel of a silicon nanotransistor and show measurable two-donor exchange coupling.[1] Moreover, the analysis of the three charge states of the molecule shows evidence of a simultaneous enhancement of the binding and charging energies with respect to the single donor spectrum. Such enhancement suggests a potential physical mechanism to increase the operation temperature of conventional single-atom transistors and improve their robustness against interfacial electric fields. The measured data are accurately matched by results obtained in an effective mass theory incorporating the Bloch states multiplicity in Si, a central cell corrected donor potential and a full configuration interaction[24] treatment of the two-electron spectrum. Early work based on EMA failed to capture the subtle effects of valley physics in silicon[25] or only the asymptotic behavior at large interdonor distances was obtained through Heitler−London method.[26] The size of the system hinders the applicability of computationally demanding full atomistic treatments.[27,28]
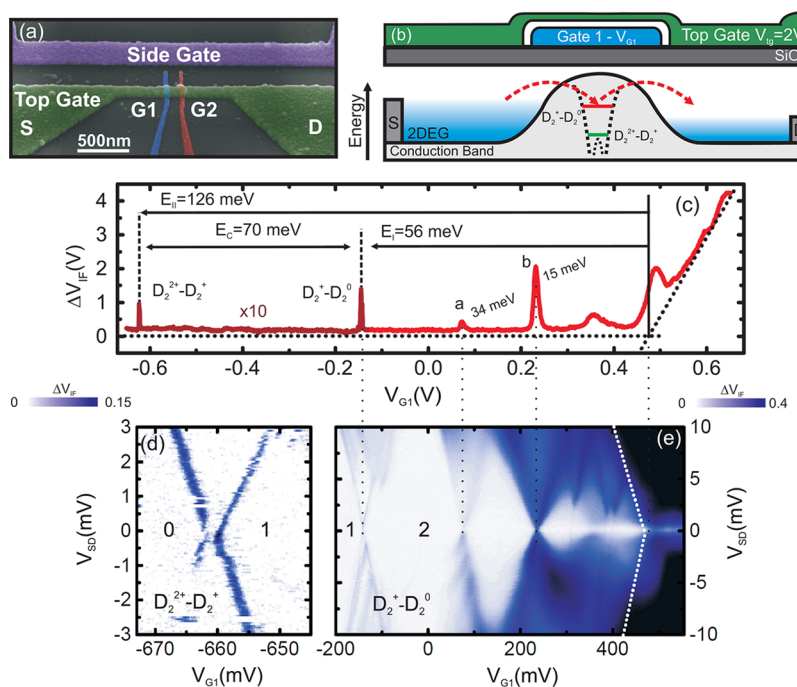
Figure 1. (a) False color scanning electron microscope image of the device. (b) Schematic cross-section of the energy bands across the relevant tunnel barrier G1 along the direction of transport indicating the potential induced by the molecule. (c) Reflectometry response V_{IF} as a function of the source barrier gate in the subthreshold regime. The signal of the (d) zero to one electron transition, $D_2^+ \rightarrow D_2^+$, and (e) of the one to two electron transition, $D_2^+ \rightarrow D_2^0$, with respect to the conduction band edge, white dotted line.

We fabricated a double-gated metal-oxide–semiconductor field-effect transistor (FET), Figure 1a, to map the energy spectrum of arsenic donors in Si.[29,30] Dopants are included by low-dose ion implantation of As; see Supporting Information. The nanoFETs gates G1 and G2 control the energy band bending of the environment immediately under it. Setting it below threshold generates a barrier and current only flows through quantum tunneling (Figure 1b). Furthermore, G1(2) tunes the electrochemical levels of the impurities; i.e., the energy required to add an extra electron to the system. Whenever one of these levels resides within the energy window of the bias voltage (centered at V_{SD}), transport through the structure can occur, and resonant tunneling current peaks appear. In order to reduce the effect of $1/f$ noise on these devices we used radio frequency reflectometry.[31] This technique probes the complex impedance of the device generating a DC output voltage V_{IF} which is proportional to the differential conductance (see Supporting Information).

Up to 12 devices measured at 4 K showed subthreshold resonances associated with individual As atoms—charging energies E_C between 23 and 37 meV, as previously reported for gated donors[13,15]—with an average of two As atoms per transistor. A single FET controlled by G1 presented resonant lines with enhanced charging and binding energies. Figure 1c shows the rf-response of this device as a function of the gate voltage (V_{G1}) measured at 200 mK. Below threshold (V_{G1} = 470 mV), obtained from a fit to the linear region of the FET, we observe a set of single donor or unintentional quantum dot lines, marked as a and b, located at 34 and 15 meV with respect to the conduction edge.[29] Notably, we observe two other lines, at −660 mV and −140 mV, signaling the presence of more tightly bound states. As argued hereupon, we may label these lines as the corresponding one and two-electron transitions in a donor molecule, $D_2^{2+} \rightarrow D_2^+$ and $D_2^+ \rightarrow D_2^0$, respectively.

We quantify these energies by measuring the characteristic Coulomb diamonds (Figure 1d and e). Conventionally a constant voltage-to-energy calibration parameter $\alpha = E_D/V_{G1}$, where E_D is the energy at the dopant site, used to obtain energy values from gate voltage changes.[10,13] However, under the considerations of the constant interaction model, this is expected to be different for different electronic occupations of the molecule as experimentally observed here. Moreover, α could vary with bias conditions[11] reducing the accuracy of this method. Instead of the conventional method, we consider the extrapolated point in V_{SD} at which the edges of the Coulomb diamonds meet. The V_{SD} axis sets an absolute energy scale, free of calibration parameters, providing an accurate way to experimentally quantify the characteristic energies of the system. In this way we first obtain the ionization energies corresponding to the strong bound states at −660 mV and −140 mV from the V_{SD} point at which the edges the diamonds meet the edge of the conduction band; see Figure 1c. Following the association of these lines with the transitions in a donor molecule, the line labeled $D_2^+ \rightarrow D_2^0$ corresponds to a first ionization energy of $E_I = 56 \pm 5$ meV, while $D_2^{2+} \rightarrow D_2^+$ to a second ionization energy of $E_{II} = 126 \pm 6$ meV. Independently, we obtain the charging energy from the extrapolated V_{SD} point where the edges of the $D_2^+ \rightarrow D_2^0$ and $D_2^{2+} \rightarrow D_2^+$ transitions meet, $E_C = 70 \pm 3$ meV.

These values are markedly larger than expected for an isolated arsenic ion in bulk silicon: $E_C^{As} = 51.71$ meV, $E_I^{As} = 2.05$ meV ($As^0 \rightarrow As^-$), and $E_{II}^{As} = 53.76$ meV ($As^+ \rightarrow As^0$).[15] It is well-known that the energy spectrum of a single dopant is modified by the presence of an interface: For gated donors a reduction in E_C due to screening effects has been experimentally observed,[8] while there is experimental evidence of an enhanced E_C in systems under quantum confinement,[32] which is very unlikely to occur for the planar geometry of our device. The possible effect of the dielectric mismatch cannot explain quantitatively in any case the
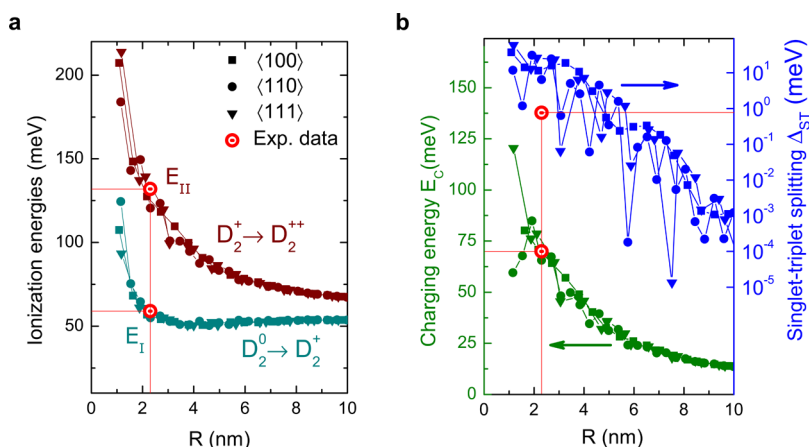
Figure 2. Calculated dependence on the interdonor distance R of (a) the first ionization energy and second ionization energy and (b) the charging energy (left) and the singlet−triplet splitting (right). The experimentally measured energies are shown (red circles) at the estimated interdonor distance $R = 2.3 \pm 0.5$ nm.
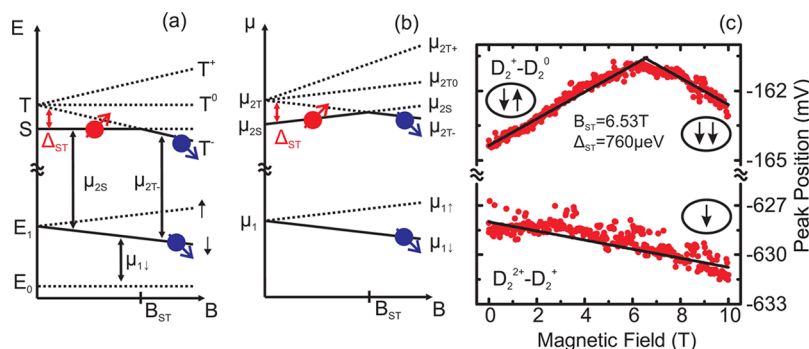

Figure 3. Schematic representation of (a) the energy evolution with field for the one-electron and the two-electron states and (b) the evolution of the electrochemical levels $\mu_{1(2)}$ as a function of magnetic field. Δ_{ST} is the singlet−triplet splitting at zero field. (c) Measured magnetic field dependence of the $D_2^+ \rightarrow D_2^+$ transition (bottom) and the $D_2^+ \rightarrow D_2^0$ transition (top) showing a singlet−triplet crossover. Black solid lines are guides to $(\pm)(1/2)g\mu_B B$.

observed energy enhancement[15] ruling out any of the aforementioned mechanism as the origin of the large energies reported here. As suggested in ref 29, the presence of As donor pairs could explain such an enhancement, as long as the donors are close enough that the electronic density is more strongly confined than it would be in a single atom. In the limit of $R \rightarrow 0$ an equivalent of the He atom will be formed, which is more confined that the H$^-$ ion and therefore has a larger charging energy. We now calculate these binding energies explicitly in order to confirm this hypothesis from the theoretical point of view.

Generalizing the hydrogenic description of isolated donors in a semiconductor environment, a donor pair may behave as a hydrogen molecule analogue. However, the molecular quantum mechanical solution only takes us so far, and a detailed understanding of the electronic structure of these molecular systems is required for the present study. A direct comparison of the measured values to a rescaled theory of H$_2$ molecules leads to inaccurate results (see Supporting Information). Calculations are performed here within an improved effective mass approach, which includes central cell corrections,[33] the full valley structure of the Si conduction band, and electron−electron correlations through a configuration interaction method. The ionization and charging energies for a donor molecule have been calculated as a function of **R**, the vector distance between the donors. The direction of **R** is relevant because of the multivalley structure of the Si conduction band. Our approach extends previous results[1,26] to much smaller distances R with higher accuracy.

The central cell correction is an empirical approximation to get the experimental ground state energy, leading to a more confined wave function compared to the plain effective mass approximation result.[33] This larger confinement implies that one and two electron binding energies calculated under the central cell corrected potential are larger than those under the plain screened Coulomb potential (Figure 2a); as a consequence, the electron−electron repulsion estimate and related quantities shown in Figure 2b are also enhanced.

Comparison between the theoretical and experimental energies leads to the identification of the measured transitions as produced by a two donor molecule with a particular interdonor distance R. We first compare the ionization energies because of the smooth behavior of these energies with R, regardless of the molecular orientation. Both E_I and E_{II} measurements, indicated in Figure 2a, are consistent with an interdonor distance of $R = 2.3 \pm 0.5$ nm. As a consequence, the charging energy is also in good agreement, even though the profile shown in Figure 2b is less accurate in determining the value of R due to its oscillatory behavior.

We may confirm the diatomic molecule nature of these states and learn about the spin configuration and the singlet−triplet splitting Δ_{ST} from the spin filling sequence of the one and two-electron energy states (Figure 3a). The exchange coupling J in the Heisenberg spin Hamiltonian $J\mathbf{S}_1 \cdot \mathbf{S}_2$—the main ingredient in CNOT operations for Kane's qubits—is determined by the singlet−triplet splitting as $J = \Delta_{ST}/\hbar^2$. Experimentally, Δ_{ST} can

be accurately identified by monitoring the evolution of the electrochemical potentials $(\mu_{1,2})$ as a function of magnetic field, in this case applied in the plane of the device (Figure 3b). Restricting ourselves to magnetic fields much smaller than the atomic unit of field $2B_0 = 65 T$, we rule out orbital effects and obtain the linear Zeeman effect as a perturbation of the atomic states, competing with the exchange coupling. The rate of change of μ in this case is given by the standard expression

$$\frac{\partial \mu_{1,2}}{\partial B_{\parallel}} = -g\mu_B \Delta S_{\parallel 1,2} \tag{1}$$

where $g \approx 2$ is the g-factor for donor-bound electrons in Si, $\mu_B = 57.8\ \mu\text{eV/T}$ the Bohr magneton, and $\Delta S_{\parallel}$ the change in total spin component along the direction of the field when an extra electron is added. Filling the molecule with a spin-down (up) electron results in a $-(+)g\mu_B/2$ slope of the chemical potential with magnetic field. In Figure 3c we measure the evolution of $\mu_{1(2)}$ as a function of magnetic field up to 10 T.

The ground state of the first loaded electron is the lower Zeeman branch; therefore the 0 to 1 electron transition shifts down as a function of field. In Figure 3c, the data are compared to a Zeeman shift $-g\mu_B/2$, calibrated to voltage shift using the lever arm $\alpha_{0\to1} = 0.21$ extracted from the slope of the edges of the $D_2^{2+} \to D_2^+$ transition. The match confirms the loading of a spin-down electron.

Experimentally the two-electron ground state Figure 3c shifts in the opposite direction at low magnetic fields, consistent with the loading of a spin-up electron and a singlet two-electron ground state at low fields. Here, we use $\alpha_{1\to2} = 0.10$ extracted from the slopes of the $D_2^+ \to D_2^0$ transition. At $B_{ST} = 6.53$ T the slope changes to $-g\mu_B/2$ indicating a change in spin configuration, a transition from spin-singlet to spin-triplet two electron ground state. From the magnetic field at which this happens, we extrapolate a zero field singlet–triplet splitting Δ_{ST} of 0.76 meV.

The small measured singlet–triplet splitting Δ_{ST} may be attributed to the particular molecule orientation leading to destructive interference of the electronic wave functions as seen in Figure 2b for the $\langle 110 \rangle$ and $\langle 111 \rangle$ crystallographic directions. This could be an example of the sensitivity of the singlet–triplet splitting to the particular positioning of donors.[26]

We investigate the robustness of these results in the presence of external electric fields since these are known to modify the single-donor spectrum.[14] Figure 4a shows the effect of a detuning electric field $E = (V_R - V_L)/R$ applied along the axis of the molecule for the distance $R = 2.3$ nm. This is accomplished by shifting the on-site energies on the molecular orbital theory by $\delta_{L,R} = -eV_{L,R}$. We disregard here the proximity of interfaces.[13,15] The separation between donors is too small for the electric field to generate a significant detuning. Moreover, the ionization energies are large due to the molecular hybridization, so that the charge states are insensitive to these external fields. This robustness explains why our theory for bulk Si describes well the energy levels even under the complex environment in our FET devices. This is an appealing feature for the scalable fabrication of donor-based transistors.

Finally, we explore theoretically a hypothetical donor-pair separation $R = 10$ nm. In this case, the existence of a classically forbidden region between the two donor sites facilitates a study of the charge occupation of each site separately. The charge stability diagram, shown in Figure 4b, is consistent with the data from Figure 2 and equivalent to the diagram in a double quantum
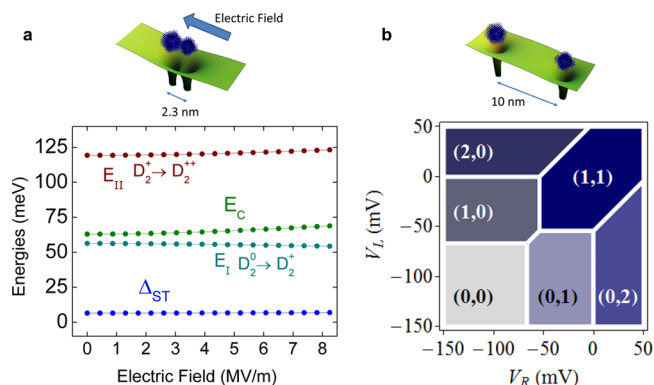

Figure 4. (a) Impact of an electric field on the spectrum of a donor pair at $R = 2.3$ nm (similar to our sample). Up to fields as high as the SiO_2 dielectric strength, the charging energies, first and second ionization energies and the singlet–triplet splitting remain essentially unchanged. (b) For $R = 10$ nm, the charge distribution is quite sensitive to external fields, as implied by the charge diagram obtained. The pair is aligned along the (110) direction in both calculations.

dot.[34] The analogy with quantum dots may be used to implement charge and spin qubits. The control over the charge degree of freedom at the $(0,1) \leftrightarrow (1,0)$ transition, instrumental for charge qubit proposals,[2] could be implemented with modest electric fields. We estimate the tunnel coupling to be $t = 210\ \mu\text{eV}$ from the gap at the level anticrossing (not shown here) around $\delta_L = \delta_R = 60$ meV.

By analogy with artificial molecules, e.g., GaAs and Si double quantum dots, one could speculate the potential of a dopant pair to be operated as a singlet–triplet spin qubit overcoming current difficulties with Kane's architecture exchange gates. This would require the demonstration of electric-field control of the exchange coupling. Such a system would have the dual advantages of enabling spin manipulation via electric, as recently demonstrated,[23] rather than magnetic fields, and the long spin coherence times of dopants in silicon. Moreover, the sample we measure here has an electron–electron spin exchange coupling J much larger than the hyperfine coupling A with the nuclei, akin to real molecules. This raises the possibility of engineering longer and more complex chains for probing quantum chemistry methods. The exchange coupling becomes comparable to the As bulk hyperfine coupling $A = 198$ MHz[35] at an interdonor distance of $R \approx 8$ nm, which sets a possible geometry for Kane's architecture.

■ ASSOCIATED CONTENT

Ⓢ Supporting Information

Device fabrication, measurement techniques, and theory. This material is available free of charge via the Internet at http://pubs.acs.org.

■ AUTHOR INFORMATION

Corresponding Authors
*E-mail: mg507@cam.ac.uk.
*E-mail: also@if.ufrj.br.

Notes

The authors declare no competing financial interest.

■ ACKNOWLEDGMENTS

■ REFERENCES

(1) Kane, B. E. *Nature* **1998**, *393*, 133−137.

(2) Hollenberg, L. C. L.; Dzurak, A. S.; Wellard, C.; Hamilton, A. R.; Reilly, D. J.; Milburn, G. J.; Clark, R. G. *Phys. Rev. B* **2004**, *69*, 4.

(3) Morello, A.; Pla, J. J.; Zwanenburg, F. A.; Chan, K. W.; Mottonen, H. H. M.; Nugroho, C. D.; Yang, C.; van Donkelaar, J. A.; Alves, A.; Jamieson, D. N.; Escott, C. C.; Hollenberg, L. C. L.; Clark, R. G.; Dzurak, A. S. *Nature* **2010**, *467*, 687.

(4) Pla, J. J.; Tan, K. Y.; Dehollain, J.; Lim, W. H.; Morton, J. L.; Jamieson, D. N.; Dzurak, A. S.; Morello, A. *Nature* **2012**, *489*, 541.

(5) Pla, J. J.; Tan, K. Y.; Dehollain, J.; Lim, W. H.; Morton, J. L.; Zwanenburg, F. A.; Jamieson, D. N.; Dzurak, A. S.; Morello, A. *Nature* **2013**, *496*, 334.

(6) Koenraad, P. M.; Flatte, M. E. *Nat. Mater.* **2013**, *10*, 91.

(7) Zwanenburg, F. A.; Dzurak, A. S.; Morello, A.; Simmons, M. Y.; Hollenberg, L. C. L.; Klimeck, G.; Rogge, S.; Coppersmith, S. N.; Eriksson, M. A. *Rev. Mod. Phys.* **2013**, *85*, 961−1019.

(8) Lansbergen, G. P.; Rahman, R.; Wellard, C. J.; Woo, I.; Caro, J.; Collaert, N.; Biesemans, S.; Klimeck, G.; Hollenberg, L. C. L.; Rogge, S. *Nat. Phys.* **2008**, *4*, 656.

(9) Fuechsle, M.; Miwa, J. A.; Mahapatra, S.; Ryu, H.; Lee, S.; Warschkow, O.; Hollenberg, L. C. L.; Klimeck, G.; Simmons, M. Y. *Nat. Nanotechnol.* **2012**, *7*, 242.

(10) Pierre, M.; Wacquez, R.; Jehl, X.; Sanquer, M.; Vinet, M.; Cueto, O. *Nat. Nanotechnol.* **2009**, *5*, 133.

(11) Sellier, H.; Lansbergen, G. P.; Caro, J.; Rogge, S.; Collaert, N.; Ferain, I.; Jurczak, M.; Biesemans, S. *Phys. Rev. Lett.* **2006**, *97*, 206805.

(12) Ono, Y.; Nishiguchi, K.; Fujiwara, A.; Yamaguchi, H.; Inokawa, H.; Takahashi, Y. *Appl. Phys. Lett.* **2007**, *90*, 102106.

(13) Tan, K. Y.; Chan, K. W.; Mottonen, M.; Morello, A.; Yang, C.; Donkelaar, J. v.; Alves, A.; Pirkkalainen, J.-M.; Jamieson, D. N.; Clark, R. G.; Dzurak, A. S. *Nano Lett.* **2009**, *10*, 11.

(14) Rahman, R.; Lansbergen, G. P.; Verduijn, J.; Tettamanzi, G. C.; Park, S. H.; Collaert, N.; Biesemans, S.; Klimeck, G.; Hollenberg, L. C. L.; Rogge, S. *Phys. Rev. B* **2011**, *84*, 115428.

(15) Calderón, M. J.; Verduijn, J.; Lansbergen, G. P.; Tettamanzi, G. C.; Rogge, S.; Koiller, B. *Phys. Rev. B* **2010**, *82*, 075317.

(16) Roche, B.; Riwar, R. P.; Voisin, B.; Dupont-Ferrier, E.; Wacquez, R.; Vinet, M.; Sanquer, M.; Splettstoesser, J.; Jehl, X. *Nat. Commun.* **2013**, *4*, 1581.

(17) Lansbergen, G. P.; Ono, Y.; Fujiwara, A. *Nano Lett.* **2012**, *12*, 763.

(18) Tabe, M.; Moraru, D.; Ligowski, M.; Anwar, M.; Jablonski, R.; Ono, Y.; Mizuno, T. *Phys. Rev. Lett.* **2010**, *105*, 016803.

(19) Roche, B.; Dupont-Ferrier, E.; Voisin, B.; Cobian, M.; Jehl, X.; Wacquez, R.; Vinet, M.; Niquet, Y.-M.; Sanquer, M. *Phys. Rev. Lett.* **2012**, *108*, 206812.

(20) Prati, E.; Hori, M.; Guagliardo, F.; Ferrari, G.; Shinada, T. *Nat. Nanotechnol.* **2012**, *7*, 443.

(21) Dupont-Ferrier, E.; Roche, B.; Voisin, B.; Jehl, X.; Wacquez, R.; Vinet, M.; Sanquer, M.; De Franceschi, S. *Phys. Rev. Lett.* **2013**, *110*, 136802.

(22) Weber, B.; Matthias, T. H.; Mahapatra, S.; Watson, T. F.; Ryu, H.; Rahman, R.; L, H. C.; Klimeck, G.; Simmons, M. Y. *Nat. Nanotechnol.* **2014**, DOI: 10.1038/nnano.2014.63.

(23) Dehollain, J. P.; Muhonen, J. T.; Tan, K. Y.; Saraiva, D. N.; Jamieson, A.; Dzurak, A.; Morello, A. *Phys. Rev. Lett.* **2014**, *112*, 236801.

(24) Kettle, L. M.; Goan, H.-S.; Smith, S. C. *Phys. Rev. B* **2006**, *73*, 115205.

(25) Miller, A.; Abrahams, E. *Phys. Rev.* **1960**, *120*, 745.

(26) Koiller, B.; Hu, X.; Das Sarma, S. *Phys. Rev. Lett.* **2001**, *88*, 027903.

(27) Zhang, G. G.; Canning, A.; Gronbech-Jensen, N.; Derenzo, S.; Wang, L. W. *Phys. Rev. Lett.* **2013**, *110*, 166404.

(28) Rahman, R.; Park, S. H.; Klimeck, G.; Hollenberg, L. C. L. *Nanotechnology* **2011**, *22*, 225202.

(29) González-Zalba, M. F.; Heiss, D.; Ferguson, A. J. *New J. Phys.* **2012**, *14*, 023050.

(30) Angus, S. J.; Ferguson, A. J.; Dzurak, A. S.; Clark, R. G. *Appl. Phys. Lett.* **2008**, *92*, 112103.

(31) Schoelkopf, R. J.; Wahlgren, P.; Kozhevnikov, A. A.; Delsing, P.; Prober, D. E. *Science* **1998**, *280*, 1238.

(32) Diarra, M.; Niquet, Y.-M.; Delerue, C.; Allan, G. *Phys. Rev. B* **2007**, *75*, 045301.

(33) Kohn, W. *Solid State Physics Series*; Seitz, F., Turnbull, D., Eds.; Academic Press: New York, 1957; Vol. 5.

(34) Hanson, R.; Kouwenhoven, L. P.; Petta, J. R.; Tarucha, S.; Vandersypen, L. M. K. *Rev. Mod. Phys.* **2007**, *79*, 1217−1265.

(35) Feher, G. *Phys. Rev.* **1959**, *114*, 1219−1244.